Integrative Biology

RSC Publishing

PAPER

View Article Online
View Journal | View Issue

Cite this: *Integr. Biol.*, 2013, **5**, 1407

Substrate curvature sensing through Myosin IIa upregulates early osteogenesis

Tugba Ozdemir,[a] Li-Chong Xu,[b] Christopher Siedlecki[ab] and Justin L. Brown*[a]

Topographical cues mimicking the extracellular matrix (ECM) have demonstrated control over a diverse range of cellular behaviours including: initial adhesion, migration, cell growth, differentiation and death. How cells sense, and in turn translate, the topographical cues remains to be answered, but likely involves interactions through interfacial forces that influence cytoskeletal structure and integrin clustering, leading to the downstream activity of intracellular signalling cascades. Electrospun fibers have shown significant success as a biomimetic topography for bone tissue engineering applications, but mechanisms by which osteoprogenitor cells translate the fiber geometry into intracellular signalling activity is only recently being examined. We hypothesized that increased cellular differentiation observed on fibrous topography is due to acto-myosin contractility and cellular stiffness *via* the small GTPase RhoA. In order to evaluate this hypothesis, MC3T3-E1 osteoprogenitor cells were grown on poly(methyl methacrylate) (PMMA) fibers of 1.153 $\pm$ 0.310 μm diameter. The elastic modulus of the cell surface was measured by atomic force microscopy (AFM) with a colloidal probe. Overall cellular stiffness was found to increase more than three-fold in osteoprogenitors adhered to a fiber, as opposed to those grown on a flat substrate. Pharmacological inhibition of RhoA signalling activity decreased cellular stiffness and cytoskeletal integrity of osteoprogenitors growing on fibrous substrates. Finally, we demonstrated not only RhoA activity through its effector Rho-associated coiled coil kinase II (ROCKII), but also Myosin IIa promotes early osteogenic differentiation, as shown by alkaline phosphatase (ALP) staining. Previous studies have demonstrated the importance of ROCKII on early differentiation. Our results shed light on mechanisms underlying geometry sensing by highlighting the role of Myosin IIa in addition to ROCKII and could ultimately contribute to scaffold design strategies.

Received 3rd April 2013,
Accepted 20th September 2013

DOI: 10.1039/c3ib40068a

www.rsc.org/ibiology

Insight, innovation, integration

We developed a synthetic extracellular matrix like fibrous scaffold to study geometry sensing mechanisms involved with fibrous topographies. The possible role of RhoA/ROCKII signaling activity was investigated resulting from cytoskeletal reorganization upon adhesion to a fiber. We demonstrated that cells undergo a series of cytoskeletal transformations that leads to increased intracellular tension and stress related signaling activity. The increased cytoskeletal tension due to crosstalk between RhoA/ROCKII and myosin IIa showed in addition to RhoA/ROCKII initiated intracellular tension, there may be other mechanisms involved in acto-myosin complex formation and focal adhesion stabilization. Our results demonstrate that this type of intracellular force generation mechanism is capable of inducing early osteogenic markers on fibrous as opposed to flat surfaces. Our study demonstrated micron sized extracellular matrix like fibers induced focal adhesion maturation potentially through decreasing the rate of disassembly as a function of only the fiber geometry and not the total adhesive area presented.

Introduction

Osteogenic regeneration involves cooperation of biochemical and biophysical factors that facilitate the healing process, however the exact mechanism linking the biophysical factors to biochemical factors remains elusive.[1,2] Surface topography is an intrinsic biophysical property that plays important roles in cellular response.[3] It is now widely accepted, based on established *in vitro* experimental models, that the initial event in how a cell senses the underlying topography is the formation of adhesive structures.[4–8] Cells form adhesions through heterodimeric integrin receptors anchoring to the surface. Integrin binding leads to a complex cascade of events resulting in the coupling of filamentous actin (f-actin) to the integrins through

[a] *Department of Bioengineering, The Pennsylvania State University, 205 Hallowell Building, University Park, PA, USA. E-mail: jlbbio@engr.psu.edu; Fax: +1 8148630490; Tel: +1 8148655190*

[b] *Biomedical Engineering Institute, Division of Artificial Organs, Department of Surgery, Mailcode: H151, Hershey Medical Center, Penn State College of Medicine, Hershey, PA, USA*

a network of proteins. The integrin mediated protein network use conformational changes (through phosphorylation and dephosphorylation) to sense and translate the external forces into the cells.[9,10] As the process advances, integrins cluster to form different types of adhesions (focal complex, focal adhesion, fibrillar adhesions, *etc.*) depending on the surface properties. Although the threshold for integrin clustering is expected to be conserved for any given substrate, external forces acting on the cell through different substrate topography could ultimately have profound effects on the integrin clusters.[11,12,42] For instance, RhoA/ROCKII initiated cytoskeletal actin remodeling and stress fiber formation was shown to respond altered topography and suggests a possible mechanism that allows cells to sense extracellular matrix fibers.[3]

The extracellular matrix (ECM) of cells composed of one of two different organizations of fibers. One takes the form of single polymer chains, *e.g.* fibronectin presenting individual nanoscale epitopes. The other embodies a highly ordered hierarchy, such as collagen and elastin fibers reaching several micron size fiber bundles, to provide both mechanical integrity and optimal topography.[13] In tissue engineering, it is important to design scaffolds with a comparable geometry of the native ECM such that stem cells could be able to recognize. The first step towards mimicking ECM is to create a fibrous structure that represents the characteristic dimensions of the native ECM fibers. One simple but robust way to create fibrous tissue engineering scaffolds is through using electrospinning.[14,15] The process involves driving a polymeric solution between a syringe needle tip and a grounded metal target through a high voltage electric field.[16,17] The resulting fibers are geometrically analogous to the fibers that exist in the ECM and thus provide an excellent experimental model system for the study of cellular response to fiber topography.[18] Fibrous scaffolds produced for osteogenic regeneration have previously reported to increase cell proliferation, adhesion and differentiation.[19,20] A recent study from our group demonstrated that cells form larger focal adhesions and increased p38 mitogen activated protein kinase (MAPK) signalling activity when they are grown on fibrous surfaces as opposed to flat surfaces.[21] Seo *et al.* also showed that altered microtopography increased RhoA mediated focal adhesion signalling, however the resulting downstream events have not been investigated.[22] We therefore propose that growth on fibrous surfaces limits the adhesion turnover and stabilizes stress fiber formation. Altered intracellular tension *via* increased f-actin through RhoA signalling ultimately impacts downstream signalling cascades.

This study investigates whether fibrous topography influences RhoA/(ROCKII)-induced osteoinduction and determines that osteogenic differentiation correlates with RhoA/ROCKII-initiated actomyosin cytoskeletal tension. We identified an increased focal adhesion maturation and acto-myosin complex formation (*via* RhoA/ROCKII signalling), stemming from a fibrous topography. Furthermore, we demonstrated that the intracellular tension generated by RhoA/ROCKII signalling governs the osteogenic differentiation on fibers not on flat counterparts. This study therefore delineates a mechanotransductive process in response to altered topography, provided by the ECM-analogous fiber architecture, and thereby contributes to a compendium of design parameters for effective scaffold geometries.

Materials and method

Electrospinning polymer fibers

Electrospinning with stationary copper target were performed in order to generate poly(methyl methacrylate) (PMMA, MW 120 000) (Sigma-Aldrich, St Louis, MO) fibrous substrates. Briefly, PMMA was dissolved in a 3 : 1 dimethylformamide (DMF) : tetrahydrofuran (THF) solution at 25% w/v and was transferred to a 5 ml glass syringe with a 25G needle (Beckton Dickinson, Franklin Lanes, NJ). The syringe was placed on a syringe pump (Harvard Apparatus, Holliston, MA) with a 6 mL h^{-1} flow rate. A 10 kV voltage was applied between the syringe needle tip and copper target. Fibers were collected on glass coverslips placed 18 cm from the needle tip, which were previously coated with 2% w/v poly(2-hydroxyethyl methacrylate), (PHEMA) dissolved in 70% v/v ethanol through spincoating at 5000 rpm for 10 seconds. PHEMA prevents cell adhesion to the glass coverslips. The desired density of fibrous mesh was generated after 2 min of electrospinning. The fiber-deposited slides were then heated twice on a 120 °C hot plate for 1 min each and UV treated for 30 minutes to sterilize prior to *in vitro* experiments. Control flat topography slides were generated through spincoating 2% w/v PMMA on glass coverslips.

Characterization of polymer fibers

The polymer fibers were characterized using scanning electron microscope (SEM, FEI Quanta 200) and atomic force microscopy (AFM). A Multimode AFM with a Nanoscope IIIa control system (Veeco, Santa Barbara, CA) was operated in tapping mode (intermittent contact) in air using Si probes with an aspect ratio of ~4 : 1 (TETRA, K-Tek Nanotechnology, Wilsonville, OR). AFM images were treated and analyzed by off-line AFM software. The average diameter (average of at least 100 measurements) of fibers was quantified through analysis of SEM images using the National Institute of Health's ImageJ software package.

Reagents and cell culture

Monoclonal antibodies (mAb) used for western blotting and Myosin IIa were purchased from Cell Signaling (Danvers, MA) unless otherwise noted. Vinculin mAb was purchased from GE Life Sciences (Pittsburgh, PA). P-MLC mAb was from GeneTex (Irvine, CA). For cytoskeletal tension inhibition experiments, Y27632 (10 μM final concentration in the culture dish) was purchased from Tocris Bioscience (Minneapolis, MN) and Blebbistatin (50 μM of final concentration in the culture dish) was purchased from Sigma-Aldrich (St Louis, MO) and aliquoted in DMSO. Cells were exposed to inhibitor treatment 30 minutes before fixation and/or lysis. As a positive control, DMSO was added to avoid noise in Y27632 and Blebbistatin results. MC3T3-E1 cells were purchased from American Type Culture Collection

(ATCC, Manassas, VA). Cells were grown on 15 cm tissue culture grade polystyrene (TCPS) culture dishes (Sigma-Aldrich, St Louis, MO) in alpha modified minimum essential medium (α-MEM) (Invitrogen, Carlsbad, CA), 10% fetal bovine serum (FBS, Atlanta Biologicals, Lawrenceville, GA), 1% penicillin–streptomycin (Pen–Strep) (Invitrogen, Carlsbad, CA) at 37 °C, 5% CO_2 with 95% humidity. When they reached 80% confluence, cells were detached from the surface using trypsin-EDTA (Invitrogen, Carlbad, CA) and either passed to culture expansion or further treatments to prepare cell suspensions for experiments.

Flat PMMA spin-coated and PMMA fibers deposited on 22 × 22 mm glass slides and after UV sterilization cells were seeded on experimental scaffold surfaces at 3000 cells per cm^2 and cultured in a mineralization medium consisting of α-MEM, 10% FBS, 1% Pen–Strep, 10 μg mL^{-1} ascorbic acid and 3 mM β-glycerol phosphate sodium salt hydrate in an incubator at 37 °C, 5% CO_2 with 95% humidity until the predetermined experimental time points for further biological assays were reached.

Cell staining

ALP activity of cells growing on substrates was tested using Sigma kit No. 85 (St Louis, MO), following the manufacturer's instructions. After completion of ALP staining, photographs of the cells were taken using a Nikon Eclipse 2000 microscope, and the ratio of ALP positively stained cells *versus* total cell number were quantified to reflect percentage of differentiation following a previously published method.[23] Immunofluorescence labelling was performed to visualize focal adhesion formation and the cytoskeletal rearrangement of cells growing on fibrous substrates in the presence or absence of cytoskeletal tension inhibitors. Briefly, cells were fixed in 3.7% paraformaldehyde followed by incubation with a permeabilization buffer (3% BSA and 0.1% Triton X-100 in PBS). Cells were then incubated in primary antibody diluted in permeabilization buffer, following the dilution ratio suggested by the manufacturer's datasheet, for 1 hour at room temperature (RT). Formation of actin fibers was detected using CF 350 conjugated phalloidin (dilution, 1 : 1000) by incubating for 30 minutes. Nuclei were stained by incubation with 4′-6-diamidino-2-phenylindole (DAPI) (1 : 5000) for 5 minutes. The stained slides were mounted using Profade Gold antifade reagent (Invitrogen, Calrsbad, CA) and imaged with a Leica DM5500B microscope using 40× objective for water immersion and 63× oil immersion objectives. Quantification of adhesion size and *in vitro* colocalization of f-actin and myosin IIa molecules was performed with NIH's ImageJ (Bethesda, MD). Adhesion length was calculated from lateral fluorescent intensity by drawing lines along the focal adhesion axis that was represented by vinculin fluorescent signal. Colocalization analysis was performed using commercially available AutoQuant Software (Media Cybernetics, Rockville, MD) by first uploading single channel f-actin and myosin immunofluorescence images. After determining the upper and lower threshold values, pearson coefficient were calculated from 6 different randomly selected regions within the cell. Images of colocalized pixels were also collected for analysis of the distribution of the colocalized pixels.

Western blotting

The relative changes in protein expression levels were examined using immunoblotting. Briefly, cells growing on experimental substrates were first washed in PBS (room temperature) and immediately transferred into new culture dishes to prevent background signal due to cell growth in culture wells. Then cells were lysed in ice cold RIPA (50 mM Tris-cl (pH 7.4), 150 mM NaCl, 1% NP-40, 0.25% Na-deoxycholate, and 1 mM PMSF) buffer containing protease and phosphatase inhibitors. Substrates were transferred into a −80 °C freezer and allowed to go through two freeze thaw cycles. Cell lysates were denatured by boiling in *LICOR* 4× protein buffer at 95 °C for 10 minutes prior to loading and running SDS-PAGE at 120 V for 2.5 hours. Proteins were transferred to a PVDF membrane at 100 V for 1 hour with circulated cooling. The PVDF membrane was blocked for 1 hour at RT in blocking buffer (1 : 1 Licor blocking buffer: TBST). Following blocking, the membrane was incubated in primary antibody overnight at 4 °C. Phosphorylation levels of *p*-myosin protein were normalized to the α-tubulin.

AFM cell indentation experiments

Preparation of AFM colloid probes. An AFM colloid probe was used to measure the elastic modulus of cells. The colloid probe was prepared as detailed previously.[24]

Cell mechanics measurements by AFM indentation

A multimode AFM with a Nanoscope IIIa control system and scanner-J (software version 5.31r1, Veeco Instruments, Santa Barbara, CA) was used to measure the mechanics of cell membranes. AFM force–volume image mode was used to reveal mechanical properties of cells by indentation over an area of 30 × 30 μm^2 under buffer solution in a fluid cell. The images produced by this mode consist of an array of position-deflection curves and a corresponding topographic map. All force maps were acquired at a scan rate of 1 Hz and piezo ramp size of 1500 nm with an array of 32 × 32 force curves. The trigger mode was set at a relative deflection threshold of 100 nm.

Data analysis

AFM force curve data were extracted from AFM files and analyzed off-line with tools developed in Matlab. The Young's modulus (E) was computed from approaching force curves using a Hertzian model with any arbitrary two points, (z_1, d_1) and (z_2, d_2), on the force curve:

$$\frac{1}{E} = \left[\frac{(z_1 - z_2) - (d_1 - d_2)}{\left(\frac{3k(1-\nu^2)}{4\sqrt{R}}\right)^{2/3} \left[(d_1 - d_0)^{2/3} - (d_2 - d_0)^{2/3}\right]} \right]^{3/2}$$

here, k is the spring constant of the cantilever, ν is Poisson's ratio, R is the radius of the tip, and d_0 is the initial deflection of the cantilever when the tip contacts the surface.[25]

Statistical analysis

All experiments were performed in triplicate and data is represented as mean ± standard deviation unless otherwise noted. Data were analyzed using MINITAB Student (version 14). The results were considered significant if the p values are equal or less than 0.05 after performing a one-way ANOVA with *post hoc* Tukey HSD test.

Results

Surface characterization and cellular stiffening on fibers

We first prepared a completely smooth surface by spin coating 2% PMMA on 22 × 22 mm glass slides. The smoothness of PMMA coated surfaces was examined by tapping mode AFM (Fig. 1A). In Fig. 1B and C, AFM height images of electrospun fiber-coated surfaces are provided. In Fig. 1B a top-view image of an individual fiber shows a flat topography underneath individual fibers which would exclude the possibility of heterogeneity in topography. In Fig. 1C a side-view AFM height image shows that, at the intersection of both fibers, each fiber individually sits on top of the other. This indicates the preservation of curved fibrous structure through the electrospinning and heat treatment processes.

The fiber diameters were measured as 1.153 ± 0.310 μm. One of the electrospinning criteria was to deposit fibers as sparse as possible in order to create a ''single layer'' of fiber mesh on top of the surface. This way we made sure the observed cellular response is due to the curved topography provided by the fibers not the disruption of cell polarity *via* providing a 3-D mesh. Additionally, limitation of the available adhesive area *via* fibers was taken into consideration, thus we tested whether available adhesive area was generating an artefact in our proposed hypothesis. For that we deposited the fibers in single and double density fashion by doubling the electrospinning time while staying in the ''single layer'' requirement as described above. Single and double density topographies were tested for RhoA activity on fibers.

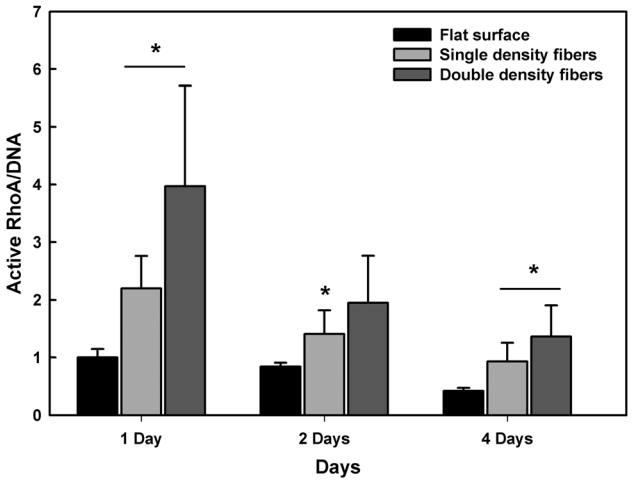

Fig. 2 Relative RhoA activity was tested on control, single density fiber coated and double layer fiber coated substrates at 1 day, 2 days and 4 days time points. The overall RhoA activity decreased as the cells reach to 4 days time point but the trend of relative differences between topography groups conserved for different time points. Although RhoA activity of fiber coated surfaces at both densities were significantly higher compared to control surfaces, the difference in RhoA activity is not statistically significant between single or double density fibers. *$p < 0.05$ compared to flat surface case at 1 day, 2 days and 4 days respectively.

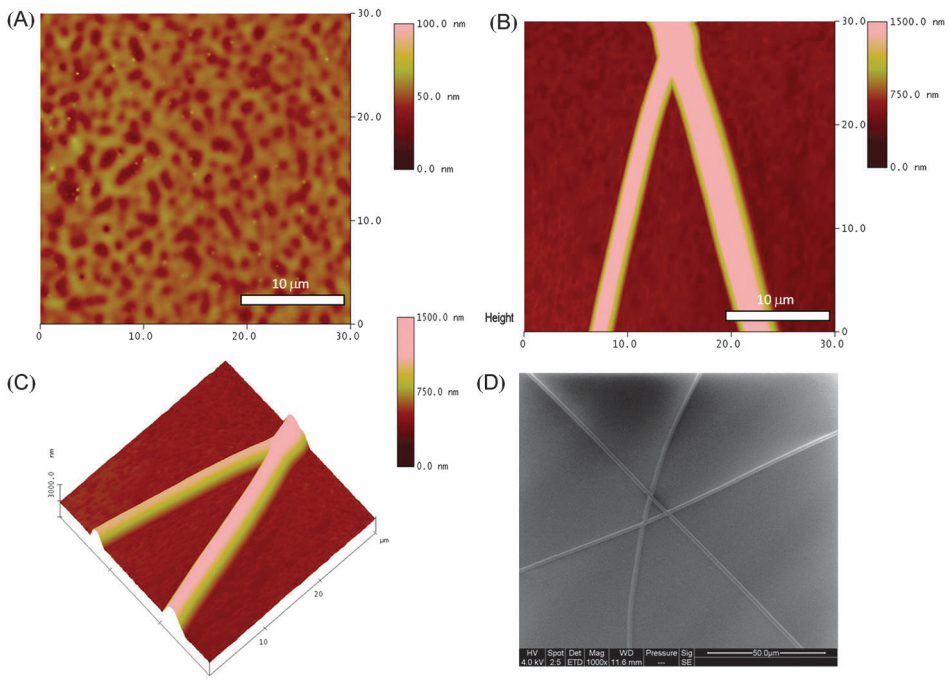

Fig. 1 AFM topographical images of 2% PMMA spin coated surfaces (A), top view (B) and side view (C) of PMMA fibers. The fibers were further imaged by SEM (1000×) to measure the diameters (n = 100) (D).

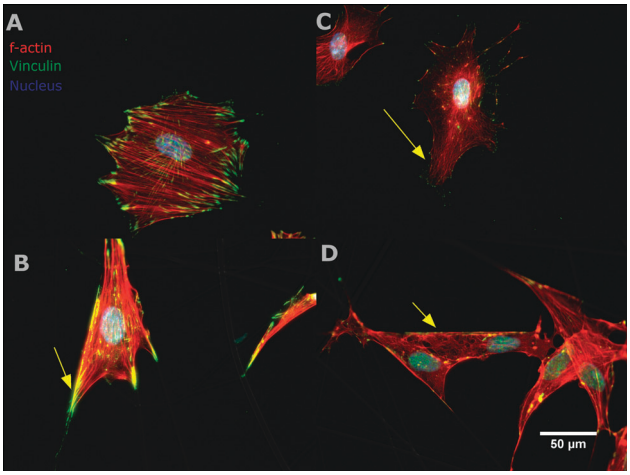

Fig. 3 Immunofluorescence imaging of cytoskeletal f-actin (red) and vinculin (green) examined to visualize the morphology of MC3T3E1 growing on flat PMMA (A and C) *versus* fibrous (B and D) surfaces. Involvement of RhoA/ROCK in cytoskeletal rearrangement (C and D) showed ROCKII inhibition of cells growing on flat PMMA (C), while fibrous PMMA (D) show a decrease in adhesion size (yellow arrows).

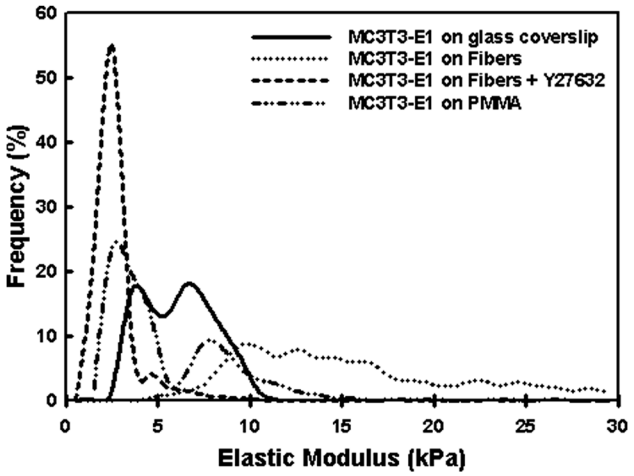

Fig. 4 Graph showing the distribution of elastic moduli of MC3T3-E1 cells growing on PMMA (two dots and dash), cleaned glass (straight line), fibers (dotted line), fibers with a ROCK inhibitor (dash line). The elastic modulus values measured are higher for MC3T3-E1 cells growing on fibrous surfaces. ROCK inhibitor Y27632 caused a dramatic decrease in overall elastic modulus (n = 3).

Fig. 2 shows that RhoA activity is more than two fold higher when cells are grown on fibrous substrates. Activity diminishes as the cells grow, on both flat and fibrous surfaces, with an approximately 60% reduction for fibrous substrates and 50% for the flat substrate. In this regard, we increased the adhesive surface area by increasing the fiber density (increased fiber deposition time) and measured the RhoA activity. Results in Fig. 2 confirm that the RhoA activity is double the RhoA activity on the less dense fiber coated surface. Next we used immunofluorescence imaging (Fig. 3) to observe the morphological changes in the actin cytoskeleton and focal adhesion maturation through targeting f-actin (red) with CF565 conjugated phalloidin, and vinculin immunolabeled with A488 (green). The first important observation was the enhanced density of vinculin fluorescence signal along the fibers where cells attach, as opposed to flat surfaces (Fig. 3B and A, respectively). Inhibition of the RhoA effector ROCKII significantly decreased the adhesion formation on both flat and fibrous surfaces (Fig. 3C and D). Although the adhesions became less visible, the smaller vinculin clusters were still observed on cells adhering to a fiber (Fig. 3D yellow arrows). We therefore propose that ROCKII inhibition-induced deficiency of adhesions would have an impact on intracellular tension, generated by cells growing on PMMA fibers.

In order to test the intracellular tension we seeded cells onto flat and fibrous substrates and measured their elastic modulus with AFM as a representative of intracellular tension. The modulus distributions of the cells growing on each substrate are illustrated in Fig. 4. The cells growing on fibers (the distribution with continuous dotted line) have a distribution presenting a higher mean and median modulus as compared to the cells growing on PMMA spin coated surfaces (dot-dash line). As a negative control we also measured the stiffness of a cell growing on a cleaned glass coverslip (solid line). Both PMMA coated and glass coverslip samples have elastic modulus distributions that are smaller than the fiber coated samples. We further investigated whether the increased stiffness is due to enhanced RhoA activity through RhoA→ ROCKII→ MyoIIa signalling, by inhibiting ROCKII activity with Y27632. Upon inhibition of ROCKII, the elastic modulus distribution values decreased to values between 0–5 kPa, less than values obtained from a cell growing on flat PMMA. The average stiffness values measured with AFM and the corresponding cytoskeletal morphology are shown in Table 1.

As reported in the Table 1, cells growing on flat PMMA surfaces have stiffness values of 5.6 kPa, which is approximately 12% lower than a cell growing on a cleaned glass surface. The difference is predicted to be due to mechanical properties of PMMA *versus* the glass since glass is a more rigid substrate. However, the stiffness of cells growing on fibrous PMMA surfaces were measure to be 13.24 kPa which is nearly 1.5 fold higher (136%) than cells growing on flat PMMA substrates. Inhibiting the RhoA/ROCKII pathway resulted in a decrease in

Table 1 Effect of RhoA/ROCKII pathway inhibition on overall cellular stiffness and cytoskeletal adhesion organization on planar *vs.* fibrous surfaces. The extent of formation of stress fibers was represented with ''+''

	MC3T3 cells growing on			
	Glass	Flat PMMA surface	PMMA fibers	PMMA fibers + Y27632
Mean stiffness (kPa) ± Stdev	6.49 ± 3.8	5.6 ± 3.6	13.24 ± 6.3	2.75 ± 1.39
Presence of stress fibers	++	++	++++	+

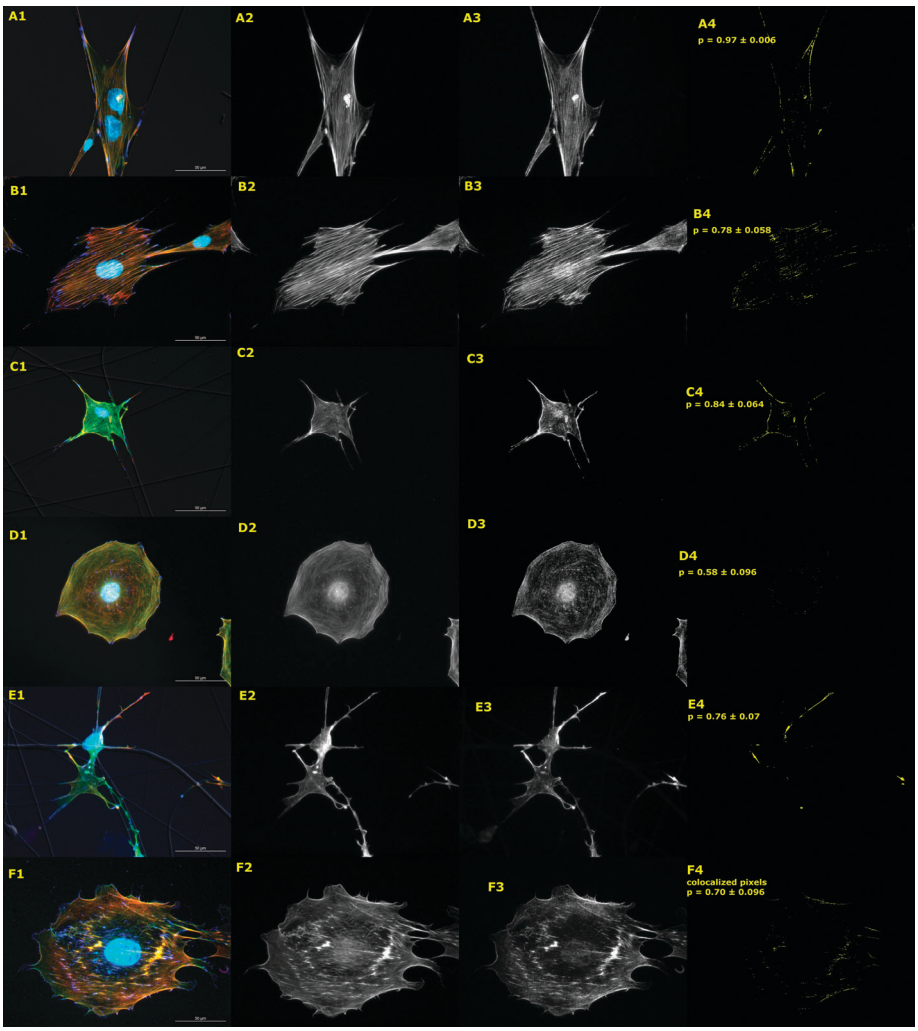

Fig. 5 Effect of RhoA activity on acto-myosin organization and focal adhesion formation of cells growing on PMMA fibers (A, C, E) and flat PMMA (B, D, F) were compared using immunofluorescence. Cells were stained for f-actin (green), myosin IIa (red) and vinculin (blue). Overlay images of f-actin and myosin IIa (the first column) show qualitative differences in cell shape and cytoskeletal feature formation on flat (B1, D1, F1) *versus* fibrous (A1, C1, E1) surfaces. In overlay pseudo-color coded images (first column) the overlap between f-actin and myosin IIa shown as yellow, overlap of f-actin, myosin IIa and vinculin shown as white, vinculin and myosin IIa overlap is shown as purple. The individual f-actin (second column) and myosin IIa (third column) images were shown as reference to overlay images and used to further quantify the colocalization. Pearson coefficients were calculated within cell boundaries show the probability of colocalization per given topography under control (A4, B4), Y27632 (C4, D4) and Blebbistatin (F4, E4) treatment respectively.

the measured stiffness values to 2.75 kPa, an approximately 80% decrease. The measured stiffness in response to RhoA/ROCKII inhibition corresponded to altered cytoskeletal morphology. In line with our immunostaining results, these results demonstrate that RhoA/ROCKII inhibition not only affect the stress fiber formation and the alignment of the adhesions with the stress fibers (Fig. 3B), but also diminishes the cellular stiffness as we treat the cells with RhoA/ROCKII inhibitor (Fig. 4).

Actin cytoskeletal reorganization through RhoA/ROCK signaling on fibers

Increased RhoA activation promotes ROCKII activity, which facilitates the activity of Myosin Light Chain Kinase (MLCK). MLCK phosphorylates non-muscle Myosin IIa to form a tension generating acto-myosin complex. However, RhoA/ROCKII/MLCK is not the only pathway leading to myosin activation and acto-myosin ratcheting. We therefore asked whether the increased stiffness values measured on AFM correspond to the cytoskeletal rearrangement observed on cells growing on fibrous substrates. The main aim of this experiment was to understand what degree of stiffness, observed on cells growing on fibers, was due to crosstalk between focal adhesions and enhanced cytoskeletal reorganizations.

In order to delineate the interplay between the formation of mature focal adhesions and stress fibers on flat PMMA *versus* PMMA fibers, we used two cytoskeletal inhibitors, Y27632 and Blebbistatin, acting on the RhoA/ROCKII pathway (Fig. 5). We used a pharmacological inhibitor of Myosin IIa (Blebbistatin) to evaluate acto-myosin contractility on the cytoskeletal integrity of MC3T3E1 cells growing on fibers as opposed to flat surfaces. An indicator of increased tension on adhesion points is overlapping

fluorescent signals between myosin IIa and f-actin fibers, which is an indicator of acto-myosin contractility. We quantitatively analyzed the overlap of fluorescent intensity profiles between f-actin stress fibers and the myosin IIa motor protein. Staining results reveal f-actin and myosin overlay on both flat and fibrous surfaces (Fig. 5A1 and B1). Inhibition of RhoA/ROCKII *via* Y27632 resulted in a loss of this colocalization (Fig. 5C1 and D1), which was most prominent in the formation of stress fibers on flat surfaces, finally myosin II inhibitor Blebbistatin destroyed not only the cytoskeletal integrity but also the cell shape on both surfaces (Fig. 5E1 and F1). The pearson coefficients reveal that there is 20% difference of colocalized pixels between fiber and flat PMMA cases and inhibition of RhoA/ROCKII pathway *via* Y27632 decouples the acto-myosin complex (Fig. 5C4 and D4). Using immunofluorescence, f-actin (Fig. 5A2, B2, C2, D2, E2 and F2) and myosin IIa (Fig. 5A3, B3, C3, D3, E3 and F3) are probed for cytoskeletal reorganization and vinculin (blue) is probed for focal adhesions. Images were taken using a 40× water immersion objective (Fig. 5). Even after Y27632 treatment, the cells observed to sustain colocalized pixels on fibrous surfaces. The colocalized pixel image of PMMA + Y27632 (D4) has a pearson coefficient of 0.58 ± 0.0096 whereas PMMA fibers + Y27632 (C4) has 0.84 ± 0.064 size. Acto-myosin colocalized pixel images demonstrated a sparse distribution on the areas not adhering to fibrous topography (Fig. 5C4) after Y27632 treatment. Immunostaining revealed that the focal adhesions are lost on both flat (Fig. 5E1) and fibrous (Fig. 5F1) surfaces, however the impact of Blebbistatin appears more drastic on cytoskeletal organization, acto-myosin colocalization, and adhesion formation on fibers as compared to those on flat surfaces (for actin Fig. 5A2–F2, for myosin IIa A3–F3 respectively). Acto-myosin formation on flat PMMA (B4, D4, F4) moderately decreased relative to the inhibitor-free control case, but the stress fibers were still observed. In contrast, myosin IIa depletion demonstrates catastrophic effects on cells growing on fibrous substrates (Fig. 5E4). Fig. 5E4 and F4 indicate that myosin IIa is required in the maintenance of cell shape and cytoskeletal integrity on fibrous substrates, which is not dependent on ROCKII as demonstrated by the inhibitor Y27632. The disparity between Myosin IIa and ROCKII on focal adhesion and cytoskeletal integrity is not present in cells growing on flat substrates (Fig. 5F4).

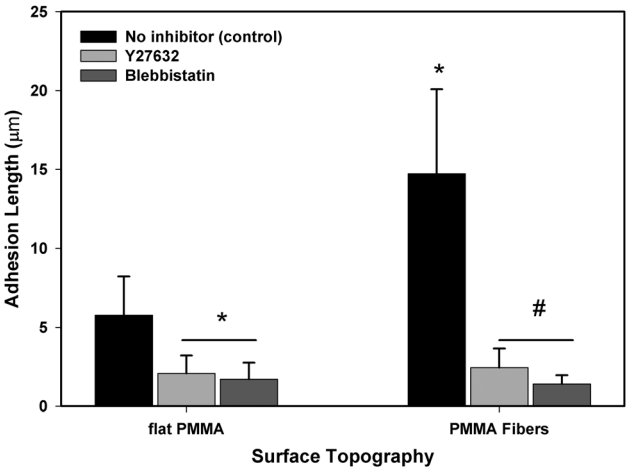

Fig. 6 The adhesion lengths were measured as a representative of focal adhesion size from fluorescent intensities of vinculin signals (n = 100 measurements) and converted into metric length units. *$p < 0.05$ compared to cells growing on flat PMMA substrates treated without inhibitor (control) case, #$p < 0.05$ cells growing on PMMA fibers treated without inhibitor (control) case.

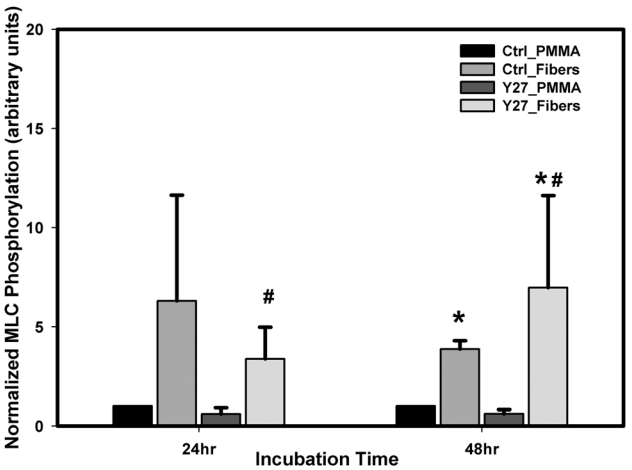

Fig. 7 Semi-quantitative western blot of MLC (myosin light chain) phophorylation is higher on cells growing on fibers 48 hours after cell seeding. Y27632 inhibition decrease phosphorylation levels on PMMA but not fibrous surfaces (n = 3) *$p < 0.05$ compared to cells growing on Ctrl_PMMA substrates, #$p < 0.05$ cells growing on PMMA fibers treated without inhibitor (control) case.

Involvement of myosin light chain phosphorylation activity downstream of RhoA/ROCK signalling

Focal adhesions were observed on both flat PMMA and fibrous substrates and their lengths were quantified. Adhesions on fibrous substrates were measured to be at least two fold larger than those on flat surfaces. Inhibition of RhoA/ROCKII signaling decreased the adhesion size to baseline levels on both flat and fibrous surfaces (Fig. 6). Next, we examined the dependence of RhoA signalling and contractility on regulating Myosin phosphorylation. We found myosin light chain phosphorylation is at least two fold higher on cells growing on fibers. The difference in myosin phosphorylation between fibers and flat substrates persisted after RhoA/ROCKII and Myosin IIa inhibition. We also observed a drastic increase in myosin phosphorylation of cells in response to Blebbistatin treatment (Fig. 7).

Effect of cytoskeletal disruption on early osteogenic differentiation

We observed significant changes in overall cell modulus in response to disruption of acto-myosin integrity and RhoA/ROCKII signaling. We therefore investigated how changes in cytoskeletal integrity would affect osteogenic differentiation. It is widely accepted that osteoblasts differentiate under externally applied force such as cyclic stretch or fluid shear. We therefore hypothesize that the increased tension and stiffness on cells growing on fibrous substrates would lead to differentiation

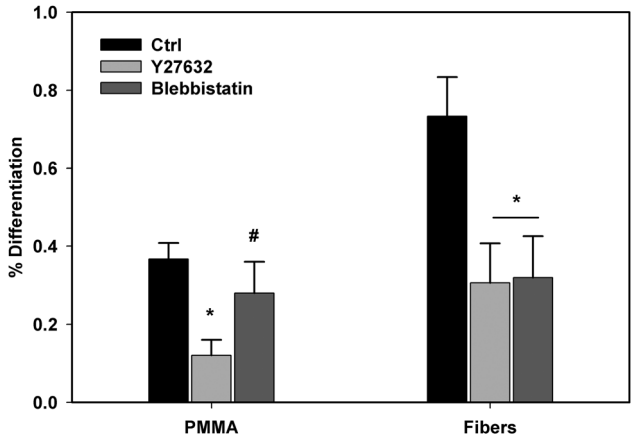

Fig. 8 Early differentiation through ALP staining quantified *via* the ratio of ALP positive stained cells per total cell number in 3 random areas in images taken by bright-field microscope. MC3T3-E1 cells growing on fibers in the presence of Y27632 and Blebbistatin were seeded on flat PMMA or PMMA fibrous surfaces and the figure indicates cytoskeletal tension-dependent ALP activity in MC3T3-E1 cells $*p < 0.05$ compared to cells growing on Ctrl treatment, $\#p < 0.05$ compared to cells treated with Y27632 ($n = 100$).

of osteoblasts. We tested the initial differentiation *via* ALP staining. Our results indicate that ALP activity is 2 fold higher when cells are grown on fibrous substrates as compared to flat surfaces (Fig. 8). Additionally, both RhoA/ROCKII and Myosin IIa inhibition decreased ALP activity more than 2 fold in cells growing on fibers (Fig. 8). The same dependency on RhoA/ROCKII was also observed for cells grown on flat surfaces, although in this case there was no dependency on Myosin IIA. The results indicate fiber mediated differentiation is a function of Myosin IIA and, by proxy, the upstream activator of Myosin IIA:ROCKII. Conversely, differentiation of cells grown on flat surfaces is a function of ROCKII alone.

Discussion

Nanofibers have proven successful in bone regenerative engineering, a field which aims to use a bottom up approach towards the generation of *de novo* tissue.[14] The bottom up approach of regenerative engineering aims to first develop a detailed understanding of cell interactions with biomaterials at the molecular level to enable the directed development of complex multicellular systems with greater success. Unravelling the molecular interactions that drive progenitor cells down desired lineages would therefore lead to improved scaffold design.[7] In osteogenic regeneration, the desired outcome would be an osteoinductive scaffold that would not require any additional growth factors to promote osteoinduction.[26] Our results demonstrated that use of fibrous topography, rather than planar surfaces, leads to an increase in osteogenesis without any additional growth factors (Fig. 6). Several other groups have also studied fibrous scaffolds for osteo-regenerative purposes.[8,19,27] For example Yoshimoto *et al.* showed that growth of rat MSCs on a nanofibrous mat promoted ECM production and multiple cell layer formation at as early as a week.[28] Another interesting study by Brown *et al.* showed introduction of a nanofibrous connective structure into a polyphosphazene microspere scaffold promoted an increase in osteoid matrix formation in a focal adhesion kinase (FAK)-dependent manner. Focal adhesion signaling and RhoA activity are known regulators of cellular contractility and stress fiber formation, suggesting a mechanism by which topographic sensing of a nanofibrous surface could occur.[29]

Activation of RhoA was recently shown to be an early indicator of osteogenic differentiation of MSCs, mechanically induced by oscillatory fluid flow.[30] Cells enhance their intracellular force transmission and tension in the presence of oscillatory fluid flow through the activation of ROCKII (a RhoA effector protein), and a subsequent increase of Runx2 expression in MSCs promotes osteoinduction. Similar to fluid flow, surface topography could also generate disturbances in tensional homeostasis through cytoskeletal reorganization.[31] Our results demonstrate that growth on PMMA fibers increase cellular tension, exhibited by a three fold increase in elastic modulus, beyond that achieved with planar PMMA surfaces. Furthermore, the presence of two markers that support mechanotransduction – vinculin for adhesion maturation anchoring the cytoskeleton, and actin stress fibers for force transmission – validate our AFM measurements. Other groups have studied the effects of nano and microscale surface features on cytoskeletal tension-mediated osteogenic differentiation. Hansen *et al.* reported that MC3T3E1 cells can sense and respond to surface topography by adjusting intracellular stiffness;[25] however they did not investigate the possible mechanism and downstream signalling cascade activity. In a recent finding by Seo *et al.*, a 2 micron distance separating 1×1 micron lattice patterns was found to enhance growth and cell survival through RhoA mediated stress fiber formation and adhesion maturation.[22] Unfortunately, they also failed to report the downstream intracellular signaling cascades associated with RhoA activation. Native extracellular matrix is a diverse combination of fibers with varying dimensions (collagen bundles with 67 nm banding periodicity),[32–36] therefore nanofibrous matrices are suitable candidates to study for clinically relevant regenerative engineering strategies.

Actin-mediated cytoskeletal integrity is associated with intracellular force transmission and topographic sensing, and several reports support the role of RhoA associated stress fiber formation and acto-myosin racheting in cellular tension.[9] In addition to current literature, here we report that acto-myosin associated cytoskeletal integrity is conserved not only *via* RhoA but perhaps also by additional mechanisms associated with maintaining acto-myosin integrity (Fig. 5). Our immunostaining results show that upon ROCKII inhibition the focal adhesions became less distinct and the stress fibers diffuse. Conversely, remaining stress fibers and adhesions suggest there is still cytoskeletal tension on fibrous substrates. Myosin IIa inhibition *via* blebbistatin, however, completely disrupted acto-myosin alignment and stress fiber formation (Fig. 5C3) and resulted in a decrease in focal adhesion size and number. We also examined the phosphorylation levels of myosin light chain to probe the relationship between RhoA/ROCKII signalling and myosin activity. Interestingly, when the myosin IIa ATPase activity is inhibited, the overall phosphorylation of myosin light chain is dramatically

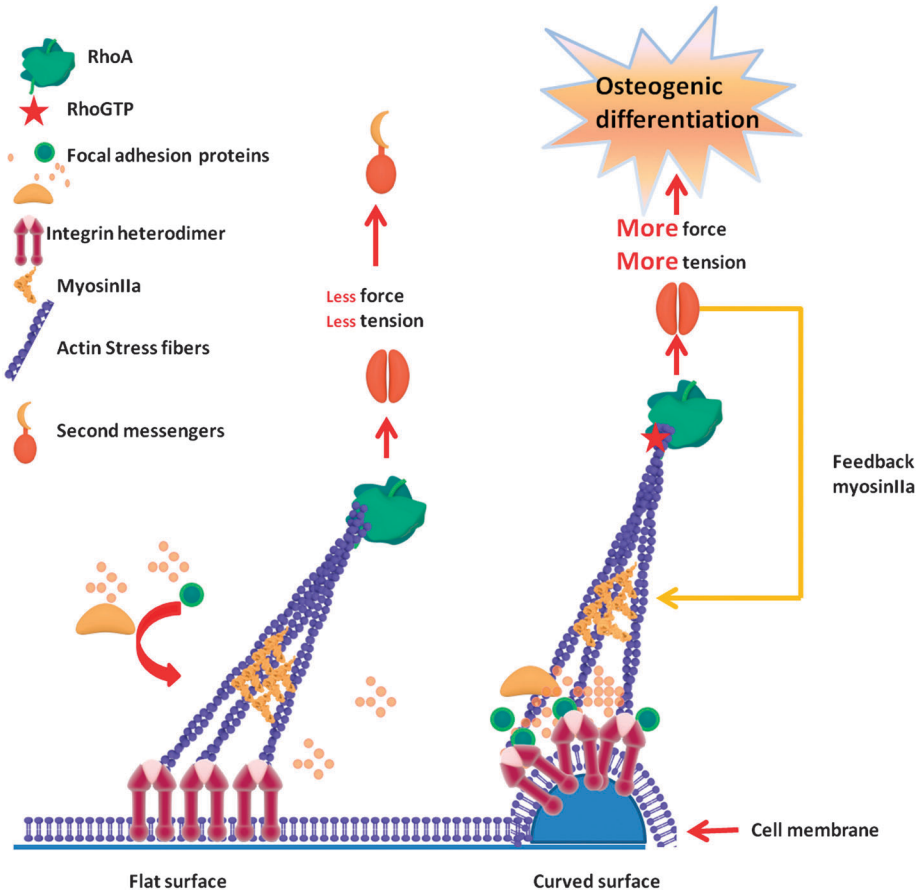

Fig. 9 The schematic of the proposed mechanism for topography sensing through RhoA/ROCK signaling. Upon adhesion, cells form adhesions through integrin receptors. Integrin receptors form clusters to generate focal adhesion protein networks. Based on the density of focal adhesion protein network densities actin stress fibers can bundle differently to a flat surface than a curved surface (such as a fibrous scaffold). RhoA was previously shown to sense and translate stress fiber density into intracellular signaling events.[38] Curved topography could potentially act on actin stress fibers such that they could facilitate RhoA/ROCKII mediated osteogenesis through enhanced Myosin IIa interactions with the actin stress fibers.

increased. Other groups also reported an enhanced myosin regulatory chain phosphorylation in response to blebbistatin treatment on adherent cells.[37] It is reported that ROCKII but not Myosin ATPase, regulates myosin regulator chain phosphorylation. These results, along with our findings, suggest a possible regulation of MLCK activity independent of RhoA/ROCKII, potentially through a decrease in Rac-1 activity, which also promotes increased MLCK activity. This is the first report of mechanisms involving the collective of RhoA/ROCKII/Myosin IIa activity and RhoA independent regulation of tensional homeostasis of osteoblasts growing on fibrous substrates.

Finally, the interactions downstream of RhoA were also investigated. The complex and interconnected protein–protein interactions collectively determine the cell fate and it is critical to determine the key regulators of a signalling response in order to predict a cellular outcome. The involvement of RhoA in topographic sensing has been studied throughout the last decade and has been shown to be essential for osteogenic differentiation.[38] Several mechanisms have been proposed by other groups for the events downstream of RhoA leading to osteogenic differentiation. One possible scenario of events is depicted in Fig. 9. In summary, when a cells faces to a curved topography the sequence of events leading to focal adhesion maturation and stress fiber formation could be due to an equilibrium of the bending energy due to curved topography, *versus* the deformation energy of the isotropic part of the cell.[39] Once activated through phosphorylation of GDP, turning into the GTP bound form, RhoA stabilizes the stress fibers and allows Myosin IIa to accumulate and create the ratcheting action that generates intracellular tension and transforms osteoprogenitors into a more osteogenic phenotype. Our previously published study[40] demonstrated the interplay between fiber scaffold diameter and MAPK (mitogen activated protein kinase) activity that might be related to adhesion-mediated cytoskeletal reorganization on fibers. In the present study we report that RhoA activity is increased on fibers, and the ability of RhoA to propagate through ROCKII to Myosin IIA is required for the enhanced differentiation observed on fibrous substrates, relative to the control. In contrast, flat surfaces demonstrate differentiation that is a function of ROCKII alone. This suggests that differentiation on flat surfaces proceeds through soluble second messenger signalling involving ROCKII, whereas differentiation on fibers proceeds through direct tension applied to the actin cytoskeleton by adhesion to the fiber.

Conclusions

In this study we investigated the role of extracellular matrix-like fiber topography on adhesion-dependent RhoA/ROCKII signalling, leading to osteoinduction. This topography-induced osteoinduction proceeds through a similar mechanism to that of tensile strain applied to a cell. Earlier reports showed[30,41] that strain promotes osteoinduction in a RhoA/ROCKII-dependent manner, and could induce autocrine BMP signalling *via* upregulation of intracellular BMP expression. We demonstrate that cells reorganize their actin stress fibers and stabilize their adhesions on fiber substrates, whereas the adhesion maturation is not as significant on planar substrates. Additionally, we demonstrate that RhoA/ROCKII signalling works in concert with Myosin IIa activation and collectively enhances cytoskeletal and focal adhesion integrity. Finally, we showed that the cellular tension generated by an acto-myosin complex facilitates osteogenic differentiation on fibrous topography without inclusion of growth factors to the media. Therefore, this study suggests that the ability of nanofibers to induce intracellular tension is a potent and intrinsic property leading to osteoblast differentiation in lieu of growth factors.

Acknowledgements

Authors would like to thank Andrew Michael Higgins for helpful discussions, and Ramdane Harouaka, Anne Kaintz for proofreading.

References

1 H. Y. Chang, J. T. Chi, S. Dudoit, C. Bondre, M. van de Rijn, D. Botstein and P. O. Brown, *Proc. Natl. Acad. Sci. U. S. A.*, 2002, **99**, 12877–12882.
2 V. Vogel and M. Sheetz, *Nat. Rev. Mol. Cell Biol.*, 2006, **7**, 265–275.
3 M. A. Schwartz and C. S. Chen, *Science*, 2013, **339**, 402–404.
4 B. D. Boyan, L. F. Bonewald, E. P. Paschalis, C. H. Lohmann, J. Rosser, D. L. Cochran, D. D. Dean, Z. Schwartz and A. L. Boskey, *Calcif. Tissue Int.*, 2002, **71**, 519–529.
5 M. J. Dalby, M. O. Riehle, D. S. Sutherland, H. Agheli and A. S. Curtis, *J. Biomed. Mater. Res., Part A*, 2004, **69**, 314–322.
6 M. J. Dalby, M. J. Biggs, N. Gadegaard, G. Kalna, C. D. Wilkinson and A. S. Curtis, *J. Cell. Biochem.*, 2007, **100**, 326–338.
7 M. Deng, R. James, C. T. Laurencin and S. G. Kumbar, *IEEE Trans. Nanobiosci.*, 2012, **11**, 3–14.
8 E. Lamers, R. van Horssen, J. te Riet, F. C. van Delft, R. Luttge, X. F. Walboomers and J. A. Jansen, *Eur. Cells Mater.*, 2010, **20**, 329–343.
9 B. Geiger, A. Bershadsky, R. Pankov and K. M. Yamada, *Nat. Rev. Mol. Cell Biol.*, 2001, **2**, 793–805.
10 M. J. Dalby, *J. Biomed. Eng.*, 2005, **27**, 730–742.
11 D. E. Ingber, *Gravit. Space Biol. Bull.*, 1997, **10**, 49–55.
12 R. O. Hynes, *Cell*, 2002, **110**, 673–687.
13 M. M. Stevens and J. H. George, *Science*, 2005, **310**, 1135–1138.
14 D. Han and P. I. Gouma, *Nanomedicine*, 2006, **2**, 37–41.
15 R. Murugan, Z. M. Huang, F. Yang and S. Ramakrishna, *J. Nanosci. Nanotechnol.*, 2007, **7**, 4595–4603.
16 W. E. Teo and S. Ramakrishna, *Nanotechnology*, 2006, **17**, R89–R106.
17 S. Liao, R. Murugan, C. K. Chan and S. Ramakrishna, *J. Mech. Behav. Biomed. Mater.*, 2008, **1**, 252–260.
18 R. Ravichandran, C. Ng, S. Liao, D. Pliszka, M. Raghunath, S. Ramakrishna and C. K. Chan, *Biomed. Mater.*, 2012, **7**, 015001.
19 J. Hu, X. Liu and P. X. Ma, *Biomaterials*, 2008, **29**, 3815–3821.
20 R. James, U. S. Toti, C. T. Laurencin and S. G. Kumbar, *Methods Mol. Biol.*, 2011, **726**, 243–258.
21 D. Jaiswal and J. L. Brown, *J. Biomed. Mater. Res., Part A*, 2012, **100**, 2921–2928.
22 C. H. Seo, K. Furukawa, K. Montagne, H. Jeong and T. Ushida, *Biomaterials*, 2011, **32**, 9568–9575.
23 Y. K. Wang, X. Yu, D. M. Cohen, M. A. Wozniak, M. T. Yang, L. Gao, J. Eyckmans and C. S. Chen, *Stem Cells Dev.*, 2012, **21**, 1176–1186.
24 X. Li and B. E. Logan, *Langmuir*, 2004, **20**, 8817–8822.
25 J. C. Hansen, J. Y. Lim, L. C. Xu, C. A. Siedlecki, D. T. Mauger and H. J. Donahue, *J. Biomech.*, 2007, **40**, 2865–2871.
26 E. S. Place, N. D. Evans and M. M. Stevens, *Nat. Mater.*, 2009, **8**, 457–470.
27 M. Deng, S. G. Kumbar, L. S. Nair, A. L. Weikel, H. R. Allcock and C. T. Laurencin, *Adv. Funct. Mater.*, 2011, **21**, 2641–2651.
28 H. Yoshimoto, Y. M. Shin, H. Terai and J. P. Vacanti, *Biomaterials*, 2003, **24**, 2077–2082.
29 J. L. Brown, M. S. Peach, L. S. Nair, S. G. Kumbar and C. T. Laurencin, *J. Biomed. Mater. Res., Part A*, 2010, **95**, 1150–1158.
30 E. J. Arnsdorf, P. Tummala, R. Y. Kwon and C. R. Jacobs, *J. Cell Sci.*, 2009, **122**, 546–553.
31 M. J. Dalby, N. Gadegaard, A. S. Curtis and R. O. Oreffo, *Curr. Stem Cell Res. Ther.*, 2007, **2**, 129–138.
32 M. Arnold, V. C. Hirschfeld-Warneken, T. Lohmuller, P. Heil, J. Blummel, E. A. Cavalcanti-Adam, M. Lopez-Garcia, P. Walther, H. Kessler, B. Geiger and J. P. Spatz, *Nano Lett.*, 2008, **8**, 2063–2069.
33 F. Jiang, H. Horber, J. Howard and D. J. Muller, *J. Struct. Biol.*, 2004, **148**, 268–278.
34 W. C. Little, M. L. Smith, U. Ebneter and V. Vogel, *Matrix Biol.*, 2008, **27**, 451–461.
35 L. A. Smith, X. Liu, J. Hu, P. Wang and P. X. Ma, *Tissue Eng., Part A*, 2009, **15**, 1855–1864.
36 M. L. Smith, D. Gourdon, W. C. Little, K. E. Kubow, R. A. Eguiluz, S. Luna-Morris and V. Vogel, *PLoS Biol.*, 2007, **5**, e268.
37 T. Watanabe, H. Hosoya and S. Yonemura, *Mol. Biol. Cell*, 2007, **18**, 605–616.
38 R. McBeath, D. M. Pirone, C. M. Nelson, K. Bhadriraju and C. S. Chen, *Dev. Cell*, 2004, **6**, 483–495.
39 Y. Y. Biton and S. A. Safran, *Phys. Biol.*, 2009, **6**, 046010.
40 D. Jaiswal and J. L. Brown, *J. Biomed. Mater. Res., Part A*, 2012, **100**, 2921–2928, DOI: 10.1002/jbm.a.34234.
41 R. D. Sumanasinghe, S. H. Bernacki and E. G. Loboa, *Tissue Eng.*, 2006, **12**, 3459–3465.
42 T. Ozdemir, A. M. Higgins and J. L. Brown, *Curr. Pharm. Des.*, 2013, **19**, 3446–3455.

